Solution structure of the cardiostimulant polypeptide anthopleurin-B and comparison with anthopleurin-A

Stephen A Monks, Paul K Pallaghy, Martin J Scanlon and Raymond S Norton*

NMR Laboratory, Biomolecular Research Institute, 381 Royal Parade, Parkville 3052, Australia

Background: The polypeptide anthopleurin-B (AP-B) is one of a number of related toxins produced by sea anemones. AP-B delays inactivation of the voltage-gated sodium channel of excitable tissue. In the mammalian heart, this effect is manifest as an increase in the force of contraction. As a result, there is interest in exploiting the anthopleurins as lead compounds in the design of novel cardiac stimulants. Essential to this endeavour is a high-resolution solution structure of the molecule describing the positions of functionally important side chains.

Results: AP-B exists in multiple conformations in solution as a result of *cis–trans* isomerization about the Gly40–Pro41 peptide bond. The solution structure of the major conformer of AP-B has been determined by two-dimensional ^{1}H NMR at pH 4.5 and 25°C. The core structure is a four-stranded, antiparallel β-sheet (residues 2–4, 20–23, 34–37 and 45–48) and includes several β-turns (6–9, 25–28, 30–33). Three loops connect the β-strands, the longest and least well defined being the first loop, extending from residues 8–17. These features are shared by other members of this family of sea anemone toxins. The locations of a number of side chains which are important for the cardiac stimulatory activity of AP-B are well defined in the structures.

Conclusions: We have described the solution structure of AP-B and compared it with that of AP-A, from which it differs by substitutions at seven amino acid positions. It shares an essentially identical fold with AP-A yet is about 10-fold more active. Comparison of the structures, particularly in the region of residues essential for activity, gives a clearer indication of the location and extent of the cardioactive pharmacophore in these polypeptides.

Structure 15 August 1995, **3**:791–803

Key words: cardiostimulant, NMR, sea anemone, sodium channel

Introduction

The polypeptides anthopleurin-A (AP-A) and anthopleurin-B (AP-B), from the sea anemone *Anthopleura xanthogrammica*, are members of a class of sea anemone toxins that interact specifically with the voltage-gated sodium channel of excitable tissue [1,2]. Not only are these polypeptides useful tools for the study of voltage-gated sodium channels, but in mammals this interaction can cause a potent positive inotropic effect• (increased force of cardiac contraction), making some of these toxins potentially useful lead compounds in the development of novel cardiac stimulants. As positive inotropes, the anthopleurins are more potent and have a higher therapeutic index than the commonly used cardiac glycoside digoxin [3]. However, they are not directly useful in cardiac therapy because they are both antigenic and orally inactive [4]. As a basis for the design and synthesis of low molecular weight agonists for use in treatment of the failing heart, a detailed knowledge of their structure and structure/function relationships is essential.

Solution structures for two type 1 [1] sea anemone toxins, AP-A [5,6] and *Anemonia sulcata* toxin Ia (ATX Ia) [7], and one type 2 toxin, *Stichodactyla helianthus* toxin I (Sh I) [8,9], have been determined using ^{1}H NMR data. The main secondary-structure element in each of these structures is a four-stranded, antiparallel β-sheet linked by three loops. The first of these loops, spanning residues 8–16 in AP-A [6], is the largest and least well defined in solution, but chemical modification studies [10,11] have shown that several residues important for activity (e.g. Asp7 and Asp9) occur in this loop. Furthermore, studies of the effect of limited proteolysis with trypsin [12] have demonstrated that the integrity of this loop is essential for the cardiac stimulatory activity of AP-A, even though it is not essential for initial binding to the voltage-gated sodium channel (LE Llewellyn and RS Norton, unpublished data).

In this paper we have determined the solution structure of AP-B, which differs in amino acid sequence from AP-A at seven positions. Of particular note are the AP-A→AP-B replacements Ser12→Arg and Val13→Pro, which might be expected to affect both the conformation and flexibility of the functionally important loop of which they are a part. Replacement of Arg12 by alanine in a recombinant analogue of AP-B [13] reduced the affinity for the neuronal sodium channel 16-fold and for the cardiac sodium channel ninefold [14], confirming that this region of the molecule is important for activity. Replacement with serine, the corresponding residue in AP-A, reduced the affinity for the neuronal sodium channel sixfold [14] but the effect on the cardiac sodium channel was not tested. Two other non-conservative substitutions in AP-B, Ser3→Pro and Thr21→Ile, occur in the β-sheet and may affect its structure. Replacement of Gln49 by lysine has only a slight effect on the affinity of the molecule for the neuronal and cardiac sodium channels [14] and, being at the end of the β-sheet, would not be expected to alter the structure. The remaining two

*Corresponding author.

 ISSN 0969-2126

substitutions (Leu24→Phe and Thr42→Asn) are conservative and are unlikely to have any significant effect on the structure. Thus, AP-B can be expected to adopt the same overall structure as AP-A but it is a more potent cardiac stimulant and its conformation is likely to be more restricted in the region of the cardioactive pharmacophore. As a reflection of this, the structure presented here provides useful new information about the nature of this pharmacophore.

Results

Resonance assignments

Amino acid spin systems were assigned using a combination of double-quantum filtered correlation (DQF-COSY) and total correlation (TOCSY) two-dimensional ^1H spectra, whereas sequence-specific assignments were made with nuclear Overhauser effect (NOESY) spectra using a standard approach [15]. Spectra at different temperatures were used to confirm connectivities in cases of peak overlap or coincidence with the water signal. Figure 1 shows the fingerprint region of a 200 ms NOESY spectrum recorded in 90% H_2O/10% ^2H_2O. Chemical shifts for the major conformer of AP-B are given in Table 1 and the sequential NOE connectivities on which the sequence-specific assignments were based, as well as other structurally relevant NMR data, are summarized in Figure 2. The conformations of peptide bonds preceding proline residues were *trans*, as indicated by strong sequential $d_{\alpha\delta}(i,i+1)$ connectivities, except for the Gly40–Pro41 bond, which has a strong sequential $d_{\alpha\alpha}(i,i+1)$ connectivity indicative of a *cis*-conformation. *Cis–trans* isomerization about the Gly40–Pro41 peptide bond was previously identified as the origin of the major conformational heterogeneity in AP-A [16]. Peak overlap in the spectra of AP-B made it difficult to confirm

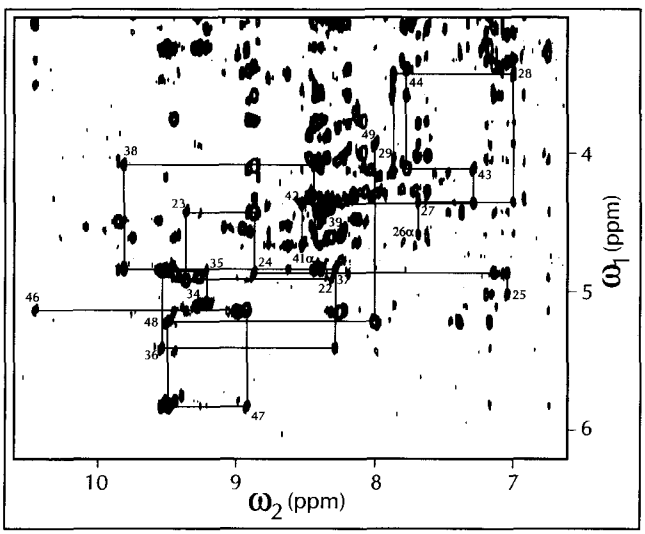

Fig. 1. Fingerprint region of a 200 ms NOESY spectrum recorded in 90% H_2O/10% ^2H_2O at pH 4.5 and 298 K, showing sequential NH–CαH connectivities for the regions 22–25, 26–29, 34–39, 41–44 and 46–49. Intra-residue connectivities are labelled with the residue number.

that the minor form adopted the *trans*-conformation, but this is what would be expected by analogy with AP-A. The spectral complexity was further exacerbated by the presence of additional minor conformers, as also observed in AP-A [16].

Structure determination and analysis

Structures were generated using a final restraint set consisting of 537 inter-proton distances inferred from NOEs, 18 backbone and 7 side-chain dihedral angle restraints and 12 stereospecific assignments for β-methylene pairs, along with 564 lower-bound restraints [6,9]. The upper-bounds restraints, from which values redundant with the covalent geometry had been eliminated, consisted of 104 intra-residue, 190 sequential, 67 medium-range ($1<i-j<5$) and 176 long-range restraints; their distribution as a function of residue number is summarized in Figure 3a. Initial structures were calculated in DIANA [17] and X-PLOR [18]. A total of 70 structures was then refined in X-PLOR by simulated annealing and energy minimization (using a modified CHARMm force-field) and the best 20 were chosen for structural analysis. A summary of geometric and energetic parameters for these structures is given in Table 2.

The root mean square differences (rmsds) for the backbone heavy atoms, when the final 20 structures are superimposed over the entire sequence, are shown as a function of residue number in Figure 3b. These data indicate that the structure is well defined except at the N terminus and around residues 8–17. The backbone angular order parameters (Fig. 3c,d) indicate that residues 18, 39, 40 and 44 are not as precisely defined as the bulk of the structure (excluding residues 8–17), but for the purpose of calculating rmsds they have been included with the well-defined residues. Thus, over residues 2–7 and 18–49 the mean pairwise rmsds for the backbone heavy atoms (N,Cα,C) and all heavy atoms are 0.64 Å and 1.11 Å, respectively. Corresponding values for the whole molecule are 2.31 Å and 3.06 Å, respectively. The β-sheet residues (2–4, 20–23, 34–37, 45–48) are very well defined, with a mean pairwise rmsd over the backbone heavy atoms of 0.46 Å.

A stereoview of the best 20 structures superimposed over the backbone heavy atoms of the well-defined residues is shown in Figure 4. The well-defined core of the molecule is clearly visible, along with the less well-defined loop connecting the first and second strands of β-sheet. The lack of definition of this loop is a reflection of the absence of long-range NOEs and the small number of medium-range NOEs to residues in this region (Fig. 3a). The loop linking the third and fourth strands of the sheet (Fig. 4), which includes the Gly40–Pro41 peptide bond, and is the site of the major conformational heterogeneity observed in the anthopleurins [16], is quite well defined in AP-B.

In a Ramachandran plot for the angular average [19,20] of the 20 refined structures of AP-B (data not shown),

Table 1. Proton chemical shifts for the major conformer of AP-B in H_2O at pH 4.5 and 298 K*.

Residue	NH	CαH	CβH	Other	Residue	NH	CαH	CβH	Other
Gly1	–†	3.39, 3.74			Ser27	7.69	4.35	*3.79, 3.93*	
Val2	8.92	4.43	2.08	$C\gamma H_3$ 0.98; 1.00	Gly28	6.99	3.43, 1.22		
Pro3		5.14	*2.39, 1.86*	$C\gamma H_2$ 2.05, 1.98; $C\delta H_2$ 4.03, 3.67	Cys29	7.87	4.04	2.48, 2.48	
					Pro30		4.00	1.37,1.37	$C\gamma H_2$ –0.10, –0.61; $C\delta H_2$ 2.35, 2.06
Cys4	8.25	4.74	3.08, 3.04						
Leu5	8.25	4.58	*1.43, 1.76*	$C\gamma H$ 1.62; $C\delta H_3$ 0.99, 0.88	Ser31	8.08	4.10	3.77, 3.77	
					Gly32	8.87	4.32, 3.58		
Cys6	8.96	4.67	3.43, 2.62		Trp33	8.39	4.84	2.99, 2.86	C(2)H 6.92;
Asp7	8.64	4.54	2.84, 2.81						N(1)H 10.32;
Ser8	8.46	4.27	4.05, 3.00						C(4)H 7.17;
Asp9	7.80	4.63	3.08, 2.90						C(7)H 7.81;
Gly10	7.61	4.26, 4.00							C(5)H 7.40;
Pro11		4.47	*2.28, 1.95*	$C\gamma H_2$ 2.00, 1.98; $C\delta H_2$ 3.69, 3.62					C(6)H 7.45
					His34	9.27	5.09	3.23, 3.23	C(2)H 8.49; C(4)H 7.16
Arg12	8.12	4.64	1.87, 1.74	$C\gamma H_2$ 1.63; $C\delta H_2$ 3.26, 3.24; $N\epsilon H$ 7.22	Asn35	9.22	4.85	3.10, 2.92	$N\delta H_2$ *7.78, 7.49*
					Cys36	9.54	5.41	*3.25, 3.46*	
Pro13		4.39	*2.30, 1.93*	$C\gamma H_2$ 2.05, 1.97; $C\delta H_2$ 3.71, 3.63	Lys37	8.28	4.84	2.00, 1.62	$C\gamma H_2$ 1.46§
					Ala38	9.81	4.08	1.32	
Arg14	8.31	4.32	1.89, 1.81	$C\gamma H_2$ 1.66, 1.63; $C\delta H_2$ 3.23; $N\epsilon H$ 7.22	His39	8.33	4.57	3.23,3.06	C(2)H 8.63; C(4)H 7.33
					Gly40	8.39	4.10, 3.55		
Gly15	8.48	4.02, 3.86			Pro41		4.66	*2.21, 2.27*	$C\gamma H_2$ 1.56, 1.52; $C\delta H_2$ 3.50, 3.32
Asn16	8.34	4.60	2.87, 2.74	$N\delta H_2$ *7.56, 6.89*					
Thr17	7.97	4.28	4.17	$C\gamma H_3$ 1.17	Asn42	8.53	4.36	2.72, 2.72	$N\delta H_2$ *7.59, 6.92*
Leu18	8.06	4.49	1.60,1.51	$C\gamma H$ 1.60; $C\delta H_3$ 0.82, 0.76	Ile43	7.28	4.11	1.75	$C\gamma H_3$ 0.90; $C\gamma H_2$ 1.43, 1.08; $C\delta H_3$ 0.84
Ser19	9.86	4.68	4.00, 3.84						
Gly20	8.39	4.83, 3.75			Gly44	7.77	3.58, 3.39		
Ile21	9.44	4.60	1.76	$C\gamma H_3$ 0.08; $C\gamma H_2$ 1.62, 1.60; $C\delta H_3$ 0.69	Trp45	8.19	4.80**	2.72, 3.06	C(2)H 7.08; N(1)H 9.42; C(4)H 7.73; C(7)H 7.43; C(5)H 7.12; C(6)H 7.22
Leu22	8.32	4.92	1.22, 1.08	$C\gamma H$ 0.98; $C\delta H_3$ 0.72, 0.69					
Trp23	9.36	4.41	*2.97, 2.84*	C(2)H 6.74; N(1)H 6.28; C(4)H 7.37; C(7)H 6.62; C(5)H 7.06; C(6)H 6.99	Cys46	10.46	5.13	3.06, 2.53	
					Cys47	8.93	5.83	3.28, 3.22	
					Lys48	9.50	5.22	1.75, 1.71	$C\gamma H_2$ 1.58, 1.53; $C\delta H_2$ 1.92, 1.89; $C\epsilon H_2$ 3.29**; $N\zeta H_3^+$ 7.33**
Phe24	8.88	4.87	*3.37, 2.69*	C(2,6)H 7.15‡					
Tyr25	7.04	5.02	*3.34, 3.14*	C(2,6)H 7.20; C(3,5)H 6.79	Lys49	8.01	3.94	*1.08, 0.73*	$C\gamma H_2$ 0.15, 0.15; $C\delta H_2$ 0.93, 0.93; $C\epsilon H_2$ 2.53; $N\zeta H_3^+$ 7.33
Pro26		4.59	*2.48, 2.07*	$C\gamma H_2$ 2.15, 2.15; $C\delta H_2$ 4.40, 3.79					

*Chemical shifts are in ppm downfield of 2,2-dimethyl-2-silapentane-5-sulfonate. For methylene groups, two chemical shifts are listed where both protons could be assigned; a single entry indicates that the degeneracy of the resonances was not determined. Resonances assigned stereospecifically are in italics, with the first entry of each pair having the lower branch number. †This resonance was not observed due to rapid exchange with solvent. ‡The C(3,5)H and C(4)H resonances are overlapped with the C(2,6)H peak at 7.15 ppm. §Connectivities to the $C\delta H_2$ and $C\epsilon H_2$ resonances were not observed at 298 K. **Observed at 285 K.

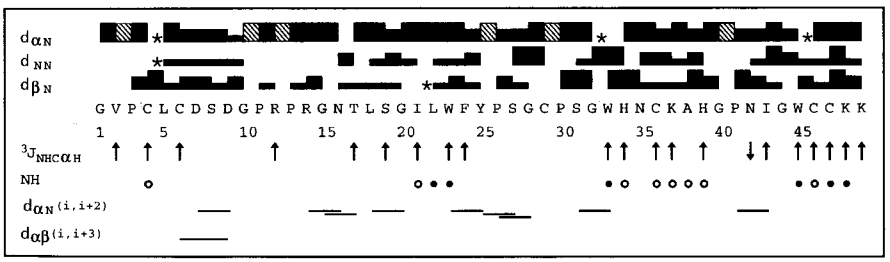

Fig. 2. Summary of sequential and medium-range connectivities for AP-B at pH 4.5 and 298 K. Filled bars indicate the sequential connectivities, with the heights of the bars indicating their strength. Medium-range connectivities are also shown, but the heights of the bars do not indicate the strength of these interactions. Hatched bars correspond to sequential $d_{\alpha\delta}$ connectivities for prolines, except for Gly40–Pro41 where a $d_{\alpha\alpha}$ connectivity was observed. A star (*) indicates that the cross-peak could not be observed due to peak overlap or water suppression. Values of ^{3}JHN-CaH>8 Hz are indicated by ↑ while values <5.5 Hz are indicated by ↓. Slowly exchanging amide protons (visible in at least two consecutive TOCSY spectra recorded after dissolution in ^2H_2O) are indicated by filled circles and those with intermediate exchange rates (visible in only the first TOCSY spectrum after dissolution in ^2H_2O) by open circles.

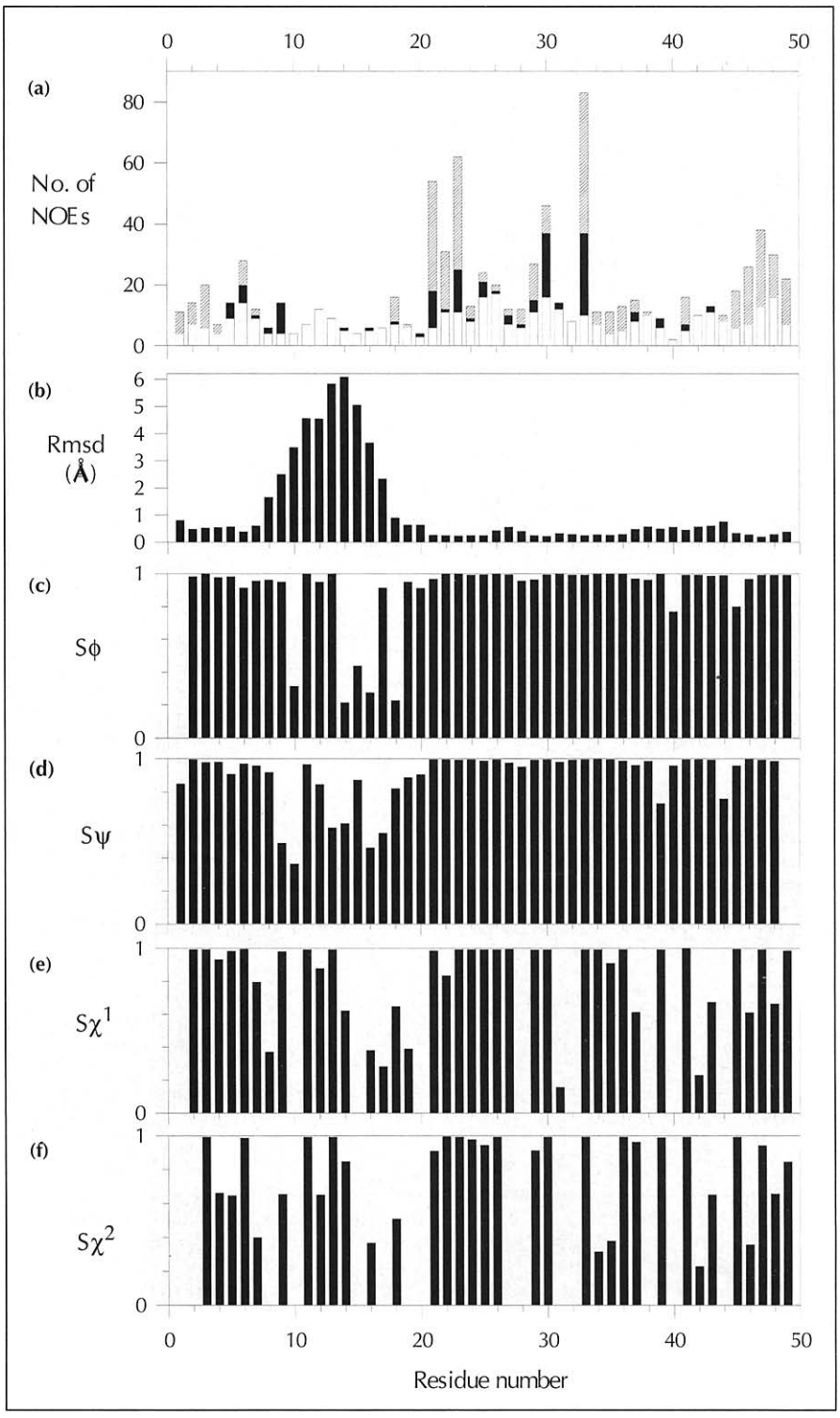

Fig. 3. Parameters characterizing the final 20 structures of AP-B, plotted as a function of residue number. **(a)** Upper-bound distance restraints used in the final round of structure refinement; long-range, medium-range and sequential connectivities are shown with hatched, black and white shading, respectively. NOEs are counted twice, once for each proton involved. **(b)** Rmsds from the mean structure for the backbone heavy atoms (N,Cα,C) following superposition over the whole molecule. **(c–f)** Angular order parameters (S) for the backbone (ϕ and ψ) and side-chain (χ^1 and χ^2) dihedral angles. Gaps in the χ^1 plot are due to glycine and alanine residues. Gaps in the χ^2 angular order plot are produced by the alanine and glycine residues. Additional gaps are introduced for residues Val2, Ser8, Thr17, Ser19, Ser27 and Ser31.

the majority of residues with well-defined backbone dihedral angles (S>0.8) fall within allowed regions. Four of the eight glycine residues and Asn35 have well-defined positive ϕ angles.

The χ^1 and χ^2 angles (Fig. 3e,f) are reasonably well defined, especially in the region of the sheet and the loop joining the second and third strands. The locations of side chains having an angular order parameter for χ^1 exceeding 0.8 are shown in Figure 5.

Description of the structure

As AP-B and AP-A differ by only seven residues, it is not surprising that their secondary structures are similar. The major secondary structural element, assigned on the basis of hydrogen-bond locations (Fig. 6) and NOEs, is a four-stranded, antiparallel β-sheet comprising residues 2–4, 20–23, 34–37 and 45–48. A β-bulge occurs in strands III and IV, with the amides of Cys36 and Lys37 forming hydrogen bonds to the carbonyl of Cys46. This bulge most closely resembles the classical C_+ subclass [21] with

Table 2. Structural statistics for 20 energy-minimized structures of AP-B from X-PLOR*.

Rms deviations from experimental distance restraints (537)†	0.015±0.0007 Å
Rms deviations from experimental dihedral restraints (25)†	0.633±0.107°
Rms deviations from idealized geometry:	
Bonds (Å)	0.0096±0.0004
Angles (°)	2.68±0.03
Impropers (°)	0.31±0.017
Energies (kcal mol^{-1}):	
E_{NOE}	14.1±1.3
E_{cdih}	0.73±0.25
E_{L-J}	−176.3±6.8
$E_{bond}+E_{angle}+E_{improper}$	144.4±3.7
E_{elec}	−539.5±14.1

*The best 20 structures after energy minimization in the distance geometry force-field of X-PLOR were subsequently energy-minimized in the CHARMm force-field, using a distance-dependent dielectric and neutralized side chains, as described in the Materials and methods section. Values in the table are mean ± standard deviation. Other details are as in [6]. †The number of restraints is shown in parentheses. None of the structures had distance violations >0.3 Å or dihedral angle violations >4°.

the residue at position 1 in the bulge (Cys36) having (ϕ,ψ) angles of (−117°,−47°) (compared with expected values of −96° and −31°, respectively) and the residue at position 2 (Lys37) having a β-sheet conformation (ϕ=−132°,ψ=125°). This classification of the bulge is supported by the fact that the amide of Cys46 forms a hydrogen bond to the carbonyl of Lys37 at position 2 in the bulge in 5 of the 20 structures.

The location of the secondary structural elements accounts reasonably well for the amide protons found to be in slow exchange with solvent (Figs 2,6). Only the amide protons of His39 and Lys48, which are slowly exchanging, lack clearly defined hydrogen-bonding partners. The most likely hydrogen-bonding partner for the amide of Lys48 is the carbonyl of His34, but this group is rotated out of the plane of the β-sheet by almost 90°. A similar twist occurs in AP-A [6], although the ψ angle of His34 and the ϕ angle of Asn35 differ between the two structures (see below). Hydrogen bonds are also found between the amides of Asp7 and Ser8 and the carbonyl of Cys36. These bonds were present in 18 and 15 of the 20 final structures, respectively, but neither amide was found to be slowly exchanging. The amide proton of Ser19 forms a hydrogen bond to the carbonyl of Cys4 in 10 of the 20 final structures, whereas the Gly20 to Cys4

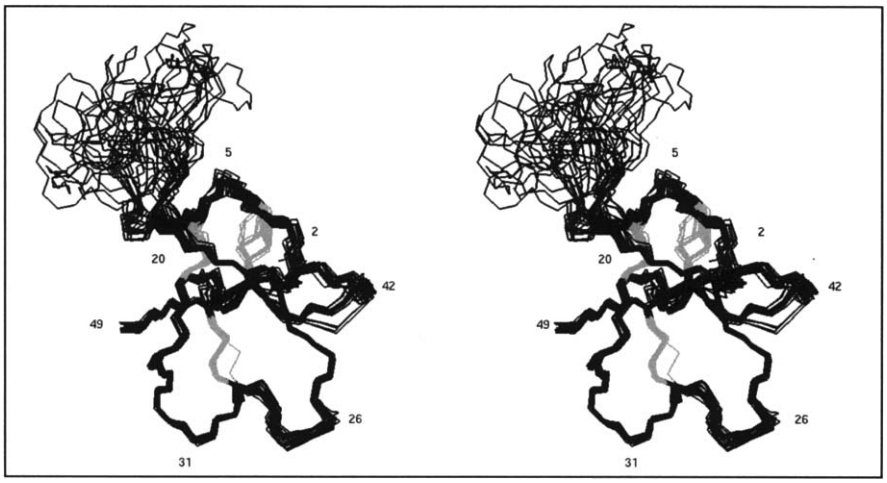

Fig. 4. Stereoview of the final 20 structures superimposed over the backbone heavy atoms (N,Cα,C) of the well-defined region encompassing residues 2–7 and 18–49. The positions of the three disulphide bonds (4–46, 6–36, 29–47) are shown in grey.

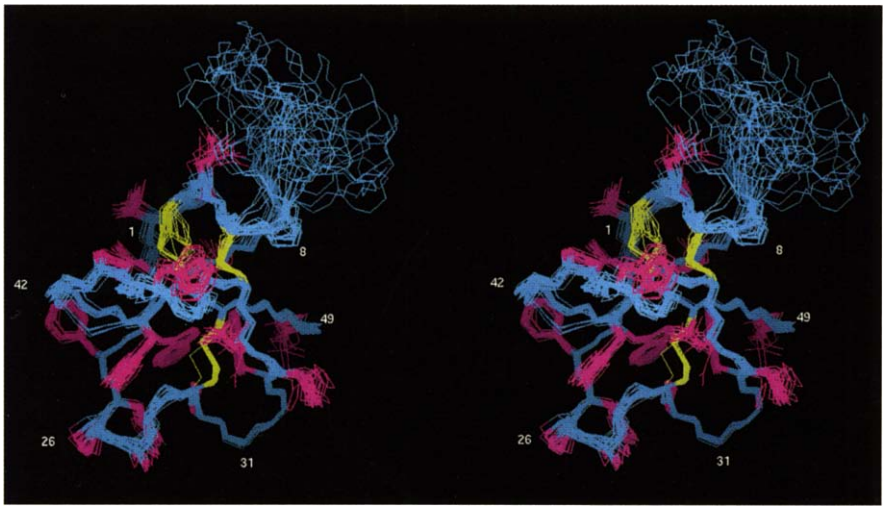

Fig. 5. Stereoview of the family of 20 final structures superimposed over the backbone atoms of residues 2–7 and 18–49. The positions of well-defined (S>0.8) side chains are shown in magenta. The disulphides are shown in yellow. This view is related to that in Figure 4 by a rotation of approximately 180° about the vertical axis.

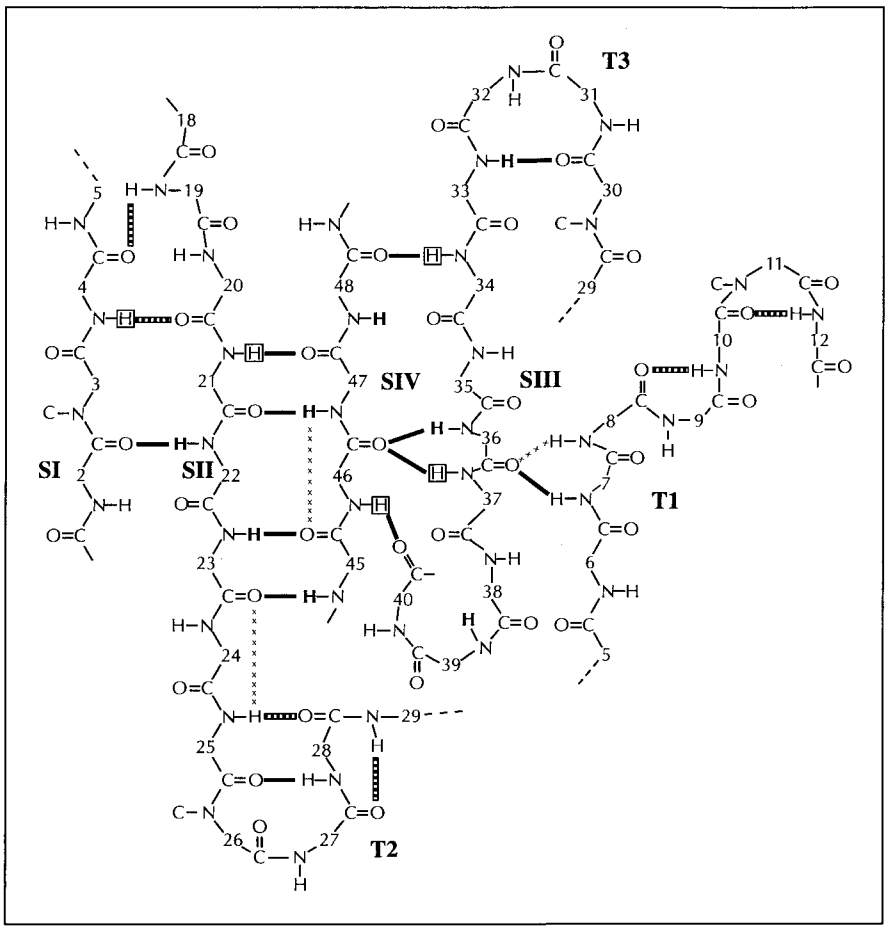

Fig. 6. Hydrogen bonding pattern in AP-B. Strands (S) I–IV and turns (T) 1–3 are labelled. Hydrogen bonds present in 18 or more of the 20 final structures are indicated by solid black bars, those present in 15–17 of the structures are indicated by crosses, and those in only 10–14 structures are indicated by striped bars. Slowly exchanging amide protons identified during the exchange experiments are shown in bold and those with intermediate exchange rates are boxed.

hydrogen bond, which is the one expected for a conventional sheet structure, is present in only three of the structures (nine in structures minimized without charge neutralization; see the Materials and methods section).

Three β-turns are present in loops linking the strands of the sheet: turn 1 (residues 6–9) is a type I β-turn (ϕ_2=–69°,ψ_2=–54°, ϕ_3=–84°,ψ_3=8°) although the 9→6 hydrogen bond is formed in only seven of the structures; turn 2 (residues 25–28) is also a type I β-turn (ϕ_2=–68°,ψ_2=–23°, ϕ_3=–92°,ψ_3=13°) with a 28→25 hydrogen bond, whereas turn 3 (residues 30–33) is a type II β-turn (ϕ_2=–51°,ψ_2=115°, ϕ_3=100°,ψ_3=–5°) with a 33→30 hydrogen bond. Additional hydrogen bonds seen in the final 20 structures but not reflected by slowly or intermediately exchanging amide protons are Gly10→Ser8 (11 structures), Arg12→Gly10 (14 structures) and Arg14→Arg12 (8 structures). Two of these, encompassing residues 10–12 (ϕ_{i+1}=–78°,ψ_{i+1}=49°) and 12–14 (ϕ_{i+1}=–73°,ψ_{i+1}=49°), resemble inverse γ-turns. All occur in the extended loop region spanning residues 8–17, a region having a higher solvent exposure than the bulk of the molecule.

The extended loop (residues 8–17) is poorly defined relative to the bulk of the molecule (Fig. 5) but is not completely disordered, being constrained locally by sequential and medium-range NOEs and two φ angle restraints. When residues 8–17 in this loop are superimposed, the mean pairwise rmsds over the backbone heavy atoms and all heavy atoms are 2.81±0.80 Å and 4.33±1.03 Å, respectively.

A number of hydrogen bonds involving side chains as donors or acceptors have also been found, as follows: Cys6 NH→Asp9 Oδ1/2 (8 structures), Asn35 Hδ22→Lys37 O (16 structures), His39 Hδ1→Ala38 O (15 structures) and Trp45 Hε1→Tyr25 O (18 structures). Most of these bonds were also present in the structures of AP-A, although with different frequencies of occurrence, with the exception of Trp45 Hε1, which was hydrogen bonded to the carbonyl of Pro26 in AP-A [6].

The disulphides 6–36 and 29–47 have χ^1 and χ^2 angular order parameters near unity and both have χ^{SS} angles of –81°. The least well defined of the disulphide bonds is the 4–46 bond: Cys4 has a well-defined χ^1 angle but a poorly defined χ^2 angle, while in Cys46 χ^1 and χ^2 are both poorly defined (Fig. 3e,f). There appear to be two major conformers present for this disulphide (Fig. 4), with 14 of the structures having a left-handed conformation (χ^{SS}=–114°) and six having a right-handed conformation (χ^{SS}=106°). Similar observations have been made for the disulphide bridges of well-defined structures of other proteins in solution, such as bovine pancreatic trypsin inhibitor [22].

Interactions between charged side chains

In the related sea anemone toxins, such as AP-A and Sh I, the carboxylate-bearing residues at positions 7 and 9 are essential for activity [1,2] and it is reasonable to expect them also to be essential in AP-B. The closest charged group to either of the aspartate side chains is the imidazolium moiety of His39. Over the final 20 structures, the average distances (mean±standard deviation) between the His39 imidazolium C2 atom and the Asp7 and Asp9 carboxylate carbons are 4.8±1.0 Å and 11.9±0.9 Å, respectively. The next closest charged group is the ϵ-ammonium group of Lys37, the distances from Lys37 Nζ atom to the Cγ atoms of Asp7 and Asp9 being 8.0±1.1 Å and 8.1±1.3 Å, respectively. The Nζ atom of Lys48 is somewhat further away, being 12.1±1.9 Å and 11.4±2.5 Å from the Cγ atoms of Asp7 and Asp9, respectively.

Discussion

The major goals of this study were to determine the structure of AP-B and to compare it with that of AP-A in order to better define the conformational space available to residues that contribute to their common cardioactive pharmacophore. As expected, the overall folds of the two molecules are essentially the same, the backbone heavy atoms (N,Cα,C) of the well-defined region (2–7,18–49) superimposing with a mean pairwise rmsd of 1.40±0.10 Å. This section focuses attention on the differences between the two structures. An important issue to be addressed in comparing the structures is whether apparent differences between them are genuine, or whether they reflect differences between the numbers of NMR-based restraints in key regions of the structure. Such differences could arise from problems of peak overlap, which were more severe in spectra of both AP-B and AP-A than would be expected for polypeptides of this size, because of the extensive peak splitting caused by conformational heterogeneity [16,23]. To begin with, therefore, we consider how differences between the calculated structures compare with differences in experimental parameters such as chemical shifts and NOEs.

Chemical shift differences

Plots of the deviations from random coil chemical shifts [24,25] for the NH and CαH resonances of AP-B and AP-A show a similar overall pattern, but local differences become evident when the differences between AP-B and AP-A are considered (Fig. 7). Protons with $|\delta_{AP\text{-}A}-\delta_{AP\text{-}B}|$ >0.1 ppm are clustered around the positions of the seven amino acid substitutions, although there are also changes in the vicinity of the aspartate residues at the start of the loop linking the first and second strands of the sheet.

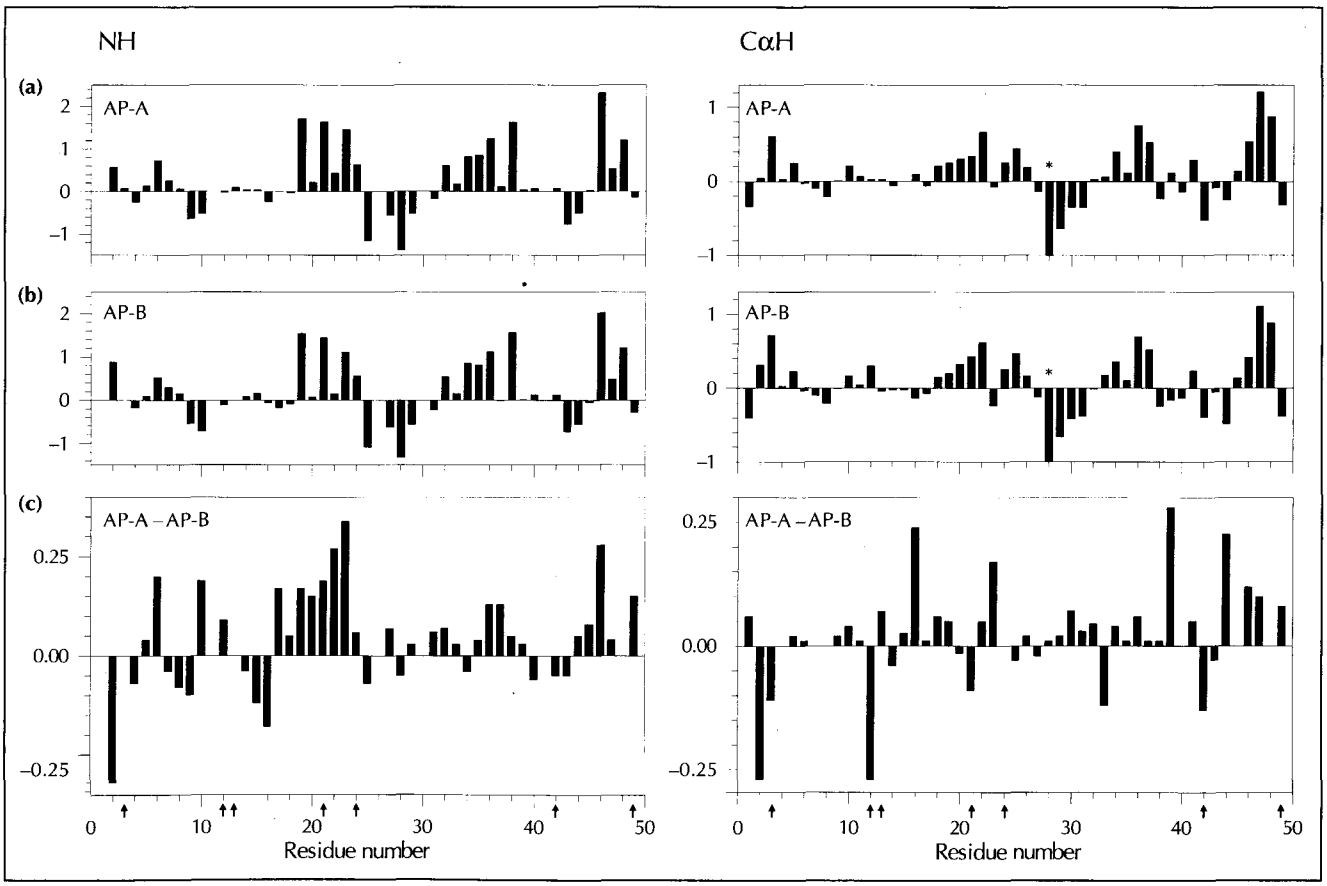

Fig. 7. Plots of deviations from random coil chemical shifts (in ppm) [25] for the NH (left) and CαH (right) resonances of AP-A **(a)** and AP-B **(b)** and for the differences between the NH and CαH chemical shifts of AP-A and AP-B **(c)**. Arrows on the horizontal axis indicate the locations of amino acid differences between AP-B and AP-A. The asterisks at Gly28 indicate that the average CαH upfield shifts in both AP-A and AP-B are off-scale at 1.6 ppm.

Differences in the first strand of the β-sheet reflect the replacement of serine by proline at position 3. Thus, the NH and CαH resonances of Val2 in AP-B are 0.32 ppm and 0.27 ppm, respectively, downfield of those in AP-A. The amide of Val2 in AP-B forms no stable hydrogen bonds, whereas in AP-A [6] it forms a hydrogen bond to the carbonyl of Leu22 in 13 of the 20 structures. The mean distances (±STANDARD DEVIATION) between the Val2 amide and Leu22 carbonyl are 4.5±0.4 Å in AP-B and 3.5±0.7 Å in AP-A. Prolines are not favoured in β-sheet structures because of their preferred ϕ angle distribution of −60±20°, but in the structures of both AP-A and AP-B the angular average ϕ angle for residue 3 is about −90°. The downfield shift of the Pro3 CαH resonance (0.72 ppm, compared with 0.61 ppm for Ser3 in AP-A) is consistent with a β-sheet environment in AP-B, the strengths of the $d_{\alpha\alpha}(3,20)$ NOEs are very similar in both spectra, and the distances between these α-protons in the calculated structures are the same (2.0±0.1 Å in AP-A and 2.1±0.2 Å in AP-B). Thus, the distortion of the first strand of the β-sheet occurs between the second and third residues in AP-B.

The amide of Cys6 in AP-B experiences less of a downfield shift than in AP-A and, unlike Cys6 in AP-A, is not in slow exchange with solvent. Cys6 from neither toxin forms stable main-chain hydrogen bonds, but a hydrogen bond to the side-chain carbonyl of Asp9 is found in 16 of 20 structures of AP-A and in only 8 of AP-B. The differences in chemical shift and exchange rates for this proton are consistent with weaker hydrogen bonding. Another difference between AP-B and AP-A in this region is in the hydrogen bonding of Ser8. In AP-B, hydrogen bonds were found to the carbonyl of Cys36 from the amide of Asp7 (18 structures) and Ser8 (15 structures) (Fig. 6), whereas in AP-A the 7→36 hydrogen bond occurred in 12 structures and the 8→36 bond did not occur in any. The amide protons of Asp7 and Ser8 were not found to be slowly exchanging in either molecule and the NH and CαH chemical shifts were unchanged between AP-B and AP-A, implying that the actual differences between the hydrogen-bonding interactions may not be as marked as implied by the calculated structures.

The titration shift (δ_B–δ_A) for the amide of Cys6 in AP-A [6] is approximately −0.57 ppm and it reflects a pK_a of about 3.0, which is closer to the less perturbed aspartate pK_a of ~3.5 than to the other aspartate pK_a of ~2 [23]. The downfield shift as the pH is raised is similar to the behaviour of the amide proton of glutamate residues in small peptides, which can form a hydrogen bond to its side-chain carboxylate that becomes stronger in the deprotonated form [26]. Hydrogen bonding with Cys6 may contribute to the reduction in pK_a of Asp9 relative to the value of 3.9 found in unstructured peptides [23]. In this case, the corresponding pK_a in AP-B, where the 6→9 hydrogen bond is less apparent, might be higher, resulting in a smaller downfield titration shift of the Cys6 amide resonance than in AP-A. Unfortunately, a previous pH titration on AP-B carried out at 300 MHz did not yield accurate pK_a values for the carboxyl groups of AP-B because the resonances broadened significantly below pH 3 (RH Fogh and RS Norton, unpublished data).

The amide resonance of Gly10 is shifted further upfield in AP-B (0.72 ppm) than in AP-A (0.53 ppm), whereas the Asp9 resonance is slightly less shifted (0.54 ppm compared with 0.64 ppm). The local interactions responsible for these perturbations do not affect the CαH chemical shifts, which are close to those typical of a random coil. In AP-B and AP-A, a 10→8 hydrogen bond is present in 11 and 7, respectively, of the 20 structures and the 9→6 hydrogen bond is present in 7 and 19, respectively. Thus, the minor changes in chemical shift appear to correlate roughly with changes in the hydrogen-bonding network in this region of the protein. In linear and cyclized synthetic peptides incorporating this region of the sequence of AP-A, the amide of Gly10 was shifted upfield by 0.18 ppm and 0.23 ppm, respectively, but the Asp9 amide had close to random coil chemical shifts [27]. In the case of Gly10, this suggests that similar structures to those in the intact proteins are populated in the isolated peptides and supports the notion that the chemical shift perturbations of Gly10 in AP-A and AP-B reflect local interactions. In the isolated peptides, the hydrogen-bonding partner for Asp9 is at the N terminus and it appears that the β-turn is destabilized as a result.

The CαH resonance of Ser12 in AP-A is at its random coil value, whereas that of Arg12 in AP-B is shifted downfield by 0.3 ppm. Although this region of both structures is less well defined, there are 12→10 and 14→12 hydrogen bonds stabilizing inverse γ-turns in 14 and 8, respectively, of the 20 AP-B structures. These hydrogen bonds were not observed in structures of AP-A. The backbone dihedral angles also differ in this region, as shown in Figure 8. There is a clear difference in the ϕ angles for residue 13, as a result of the Val→Pro substitution, and there is a large difference in the ψ angles for Pro11. Thus, as expected from the amino acid substitutions at positions 12 and 13, there are local changes in the structure of the loop in this region.

The amide of Asn16 in AP-B has a random coil chemical shift, whereas in AP-A this resonance is shifted upfield by 0.24 ppm. In AP-A, a 16→13 hydrogen bond is present in 10 of the final 20 structures and stabilizes a type II β-turn, but this bond is present in only three of the final 20 structures of AP-B, which is consistent with the difference in the amide chemical shift. The amide of Thr17 is shifted upfield slightly in AP-B (by 0.18 ppm) but not in AP-A; it does not form stable hydrogen bonds in either protein.

The overall structure of the β-sheet is similar in AP-B and AP-A although the N-terminal strand is affected by the Ser3→Pro substitution. In AP-B, the amide resonances of residues 19–23 have reduced downfield shifts compared with those in AP-A (Fig. 7), possibly indicating a slight reduction in the strength of hydrogen bonds to the second

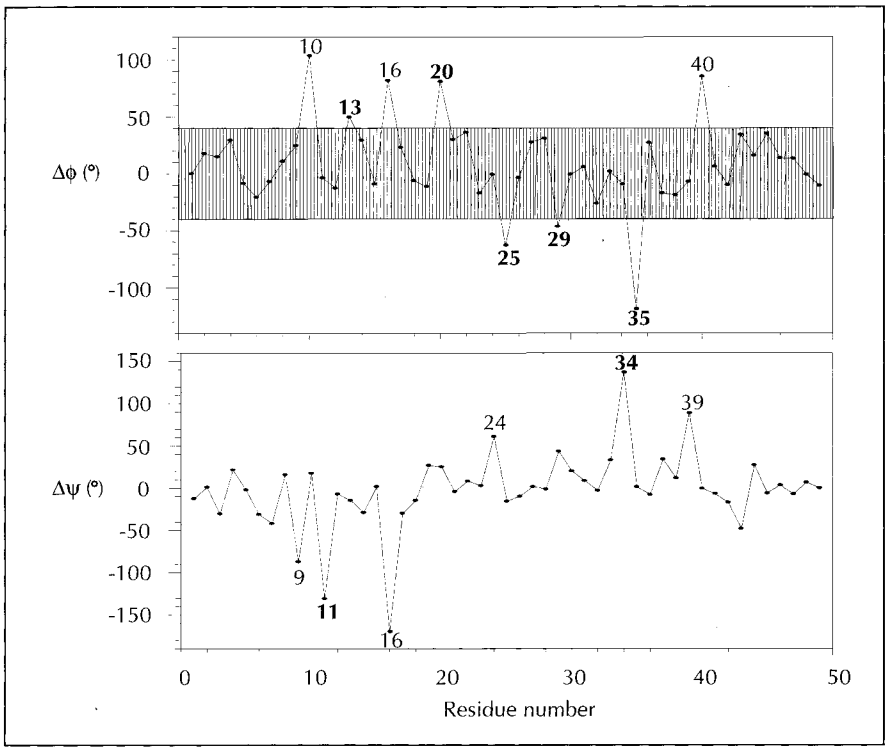

Fig. 8. Plots of the differences in backbone φ and ψ angles between AP-A and AP-B. Residues in AP-B with well-defined backbone angles are shown in bold. The shaded area represents a range of ±40° from the values to which the angles were constrained.

strand of the sheet due to the Ser3→Pro and Thr21→Ile substitutions. Both of these substitutions introduce bulkier residues with lower β-sheet-forming tendencies [28], although there is the possibility of favourable hydrophobic interactions between the new side chains.

A 19→4 hydrogen bond was present in 10 of the AP-B structures but only two of the AP-A structures. This hydrogen bond could explain the large downfield shift of the amide resonance of Ser19; the fact that similar downfield shifts are observed for both molecules suggests that the structures may be fairly similar. The possibility of local conformational disorder in this region of the structure has been discussed for ATX Ia [7] and AP-A [6], and it is likely that a similar situation prevails in AP-B. Structures containing hydrogen bonds from the Ser19 amide to the Cys4 carbonyl and from the Cys6 amide to the side chain of Asp9 are likely to be present in all three proteins and to contribute to the downfield shifts of the amide protons of Ser19 and Cys6.

The β-bulge involving residues 36, 37 and 46 appears to be better formed in AP-B, with the expected 46→37 hydrogen bond appearing in five structures. Furthermore, the 46→40 hydrogen bond in AP-B appears in 19 of the AP-B structures but only in 12 of the AP-A structures. Notwithstanding, the amides of residues 36, 37 and 46 are shifted downfield to a lesser extent in AP-B than in AP-A and these amides all exchange more quickly in AP-B than in AP-A. Thus, the better definition of the structure of AP-B compared with AP-A in this region may be a reflection of the more complete NMR restraint set for AP-B, with both the chemical shifts and exchange rates implying that the local structure of AP-B is in fact somewhat more flexible than in AP-A. More generally, the amide exchange rates for AP-B were faster than for AP-A at the same temperature and pH, implying a less rigid structure for AP-B. Changes in the CαH chemical shifts of His39 and Gly44 (Fig. 7) reflect slight changes in the Pro41-containing loop, presumably due to the substitutions at residues 24 and 42.

NOE differences

Differences between the patterns of NOE connectivities for AP-B and AP-A are a further indication of genuine structural differences between the two molecules. In the type I β-turn involving residues 6–9, the amide of Asp9 in AP-A, but not in AP-B, shows NOEs to both β-protons of Cys6. This implies that the β-turn is more stable in AP-A than in AP-B, which is consistent with the calculated structures. As noted above, the amide of Cys6 is also hydrogen bonded more strongly to the side-chain carboxyl of Asp9 in AP-A than in AP-B. The amide of Cys6 shows an NOE to the amide of Gly20 in AP-A but not AP-B. The backbone dihedral angles for these residues are well defined in both molecules (Fig. 3), but in AP-B Gly20 has a positive φ angle (average +179°), while in AP-A it is negative (average −99°; Fig. 8), pointing to a further difference in the backbone in this region. Differences in the interaction of the 6–9 β-turn with the third strand of the sheet are also apparent from the NOEs, with a $d_{N\alpha}(7,36)$ NOE present only in AP-A and a $d_{N\alpha}(8,37)$ NOE present only in AP-B. The latter NOE supports the presence of the 8→36 hydrogen bond found in AP-B but not AP-A.

The type I β-turn encompassing residues 25–28 adopts similar structures in both proteins, although when the

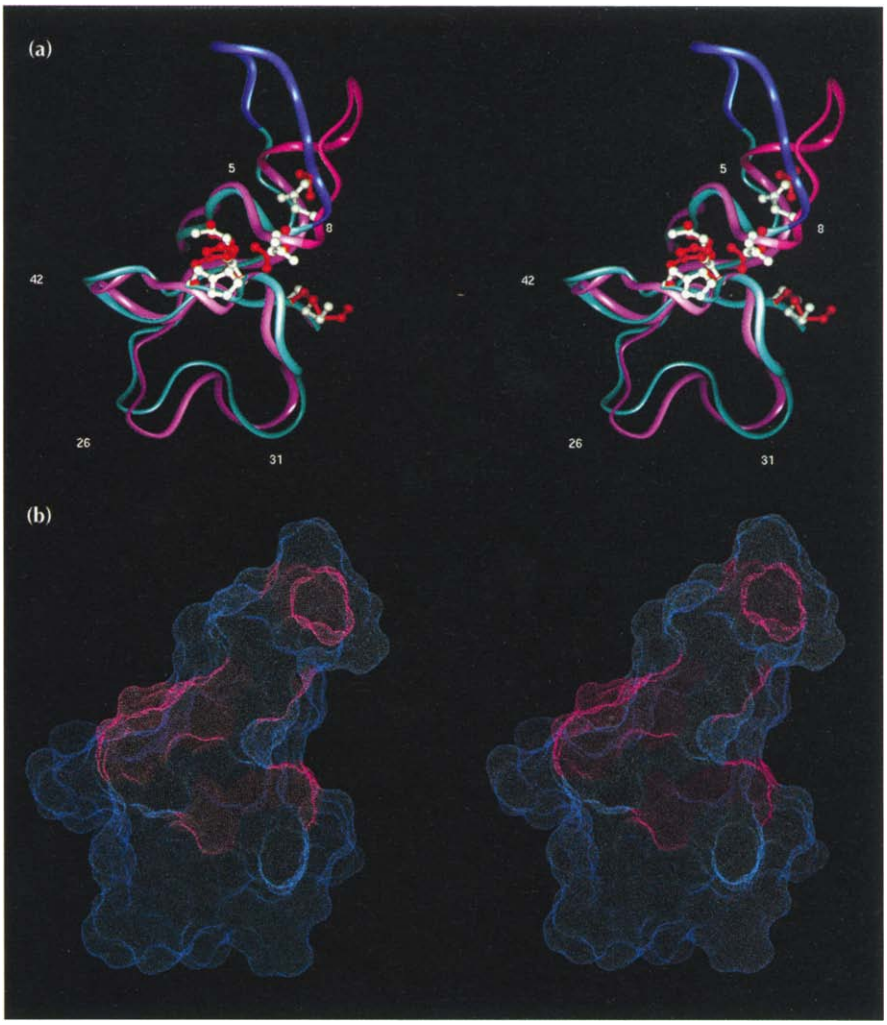

Fig. 9. (a) Stereo ribbon diagrams of superpositions of the structures of AP-B and AP-A. For each molecule, the structure closest to the geometric average is shown. Structures were superimposed over the backbone heavy atoms of residues 2–7 and 18–49, corresponding to the well-defined region of AP-B. Colours are as follows: mauve/pink indicates the well-defined region of AP-B, magenta the poorly defined loop; turquoise indicates the well-defined region of AP-A, purple the poorly defined loop. The side chains of Asp7, Asp9, Lys37, His39 and Lys48 are shown in white in AP-B and red in AP-A. **(b)** Stereoview of the structure of AP-B closest to the geometric average and showing the positions of some of the residues (Asp7, Asp9, Arg12, Asn35, Lys37, His39 and Lys48 coloured magenta) thought to contribute to the receptor-binding surface of the molecule (see text). A Connolly surface generated with a probe radius of 1.4 Å is shown; the orientation of the molecule is the same as in Figure 5.

structures are superimposed over residues 2–7 and 18–49 (Fig. 9a) it is evident that there are differences in the orientation of this turn relative to the rest of the molecule. This is a consequence of changes in the backbone dihedral angles at residues 25 and 29 (Fig. 8). In addition, the amide of Tyr25 participates in hydrogen bonds to the backbone carbonyls of Trp23 and Gly28 in AP-B but not in AP-A, although it was not found to be slowly exchanging in AP-B but was in AP-A (an amide peak at 6.95 ppm, observed in spectra of AP-A in ^2H_2O [29], has contributions from both Tyr25 and Gly28). The amides of Tyr25 and Gly28 are shifted upfield in spectra of both proteins, but to similar extents (Fig. 7). A $d_{\alpha N}(26,28)$ connectivity is observed in AP-B but not in AP-A.

In AP-A, CβH, CγH and CδH of Lys37 were constrained to be within 4.2 Å, 5.5 Å and 4.7 Å, respectively, of CβH of Cys46, and CβH and CγH were constrained to be within 5.1 Å and 5.5 Å of the Cys46 amide. These NOEs were not found in spectra of AP-B and it appears that these cross-peaks may involve other protons and were mis-assigned in the spectra of AP-A. Fortunately, in AP-A structures calculated without these restraints the respective distances are all less than those imposed by the AP-A restraints, so it appears that they have not contributed to structural differences in this region.

Finally, spectra of AP-B recorded in ^2H_2O showed NOEs between CαH of Cys36 and the side-chain protons (CβH, CγH and CδH) of Lys48. These were not present in spectra of AP-A in ^2H_2O but their effect on the structure is minor as the side chain of Lys48 is in a similar environment in both molecules (Fig. 9a). Other notable differences between the NOEs observed in ^2H_2O spectra are those from CαH of Asp7 and Lys37 to the imidazolium C(2)H of His39, which are present in AP-B but not AP-A. These NOEs reflect genuine differences between the locations of these side chains (Fig. 9a), as discussed below.

The cardioactive pharmacophore

Roles in the cardiac stimulatory activity of AP-A have been demonstrated for one or both side-chain carboxylates of Asp7 and Asp9 and one or both ϵ-ammonium groups of Lys37 and Lys48, as summarized in [6]. The contributions of the imidazolium rings of His34 and His39 are less clear, but the side chain of Arg14 appears not to be essential for stimulatory activity [6,30]. In AP-B, Arg14, Lys48 and Lys49 make only minor

contributions to activity but Arg12 appears to be important [14,31]. The locations of some of these key side chains are shown for AP-A and AP-B in Figure 9a.

In AP-A, the charged groups of Asp7 and Lys37 are within 4 Å of one another and the side chains of His39 and Asp9 are nearby. Lys48 is on the same surface of the protein but separate from the Asp7/Lys37/His39 cluster and Asp9. It is clear from a comparison of the chemical shifts, amide exchange rates and NOEs involving residues 6–9 that the type I β-turn encompassing these residues is less well formed in AP-B than in AP-A and that there are differences in the interactions between this turn and the β-sheet (as reflected by the presence of an 8→36 hydrogen bond in AP-B but not AP-A). Therefore, the locations of some of these functionally important side chains are altered in AP-B. The ammonium group of Lys37 is further from Asp7 than in AP-A and a similar distance from Asp9, whereas His39 is closer to Asp7 but still some distance from Asp9. The side chain of Arg12 is a considerable distance away from all of these groups. In AP-B, the side chain of Asn35 is closer to the Asp7/Lys37/His39 region and its side-chain amide forms a hydrogen bond to the backbone carbonyl of Lys37 in 16 of the structures. This residue is conserved throughout the type 1 toxins but is replaced by lysine in the type 2 toxins [1,2]. Evaluation of its role in the structure and cardiotonic activity of AP-A and AP-B must await the outcome of site-directed mutagenesis studies.

On the basis of crystallographic studies of peptide–protein and protein–protein complexes, the size of the surface area buried in such interactions is in the range 400–1400 $Å^2$ [32]. In the case of the potassium channel blocker charybdotoxin, 5–8 residues with surface areas of 530–850 $Å^2$ were found to be essential for binding, depending on the type of potassium channel investigated [33,34]. In AP-B, the side chains of Asp7, Asp9, Lys37, His39 and Lys48 individually contribute about 300 $Å^2$ to the solvent-accessible surface area (Fig. 9b). If Arg12 and Asn35 are also included this area increases to about 400 $Å^2$. By analogy with other protein–protein interactions, it is likely that the sodium channel binding surface of the anthopleurins will include side chains that mutagenesis studies will fail to identify as having a significant role in binding or activity. For example, alanine-scanning mutagenesis of residues in the human growth hormone–receptor interface indicated that less than 25% of the contact residues provided most of the binding energy [35]. Thus, we believe that these residues (coloured magenta in Fig. 9b) will contribute to the sodium channel binding surface of the anthopleurins by virtue of their location on the protein surface in the immediate vicinity of residues that are known to be important for activity. Other residues, as yet unidentified, may also contribute. The key requirement now is to identify those residues that provide the majority of the binding energy and to differentiate them from those whose primary role is to maintain the binding residues in the active conformation.

Biological implications

The sea anemone *Anthopleura xanthogrammica* produces two polypeptide toxins, anthopleurin (AP)-A and AP-B, which exhibit potent positive inotropic activity (i.e. increased force of cardiac contraction) *in vitro* and *in vivo*. These toxins are more active and have a higher therapeutic index than digoxin, which is still widely used for the treatment of heart failure. While the anthopleurins therefore represent useful leads in the search for alternatives to digoxin, their polypeptide nature makes them antigenic and difficult to administer, thus preventing their use as therapeutic agents.

We have determined the three-dimensional structure of the 49-residue polypeptide AP-B in solution and undertaken a detailed comparison with the structure of AP-A, from which it differs at seven residues. The structure consists of a twisted, four-stranded, antiparallel β-sheet cross-linked by three disulphide bonds. The β-sheet strands are linked by three loops, the first and largest of which is less well defined by the NMR data than the bulk of the structure. This loop contains several residues known from chemical modification and site-directed mutagenesis studies together with comparison of natural homologues to be important for the activity of the anthopleurins. Although the overall structures of AP-B and AP-A are very similar, there are differences near the start of this loop and in surrounding residues. Taking both structures together, it is possible to extend our picture of the sodium channel binding surface of these molecules, which appears to be centred on the region of Asp7, Asp9, Asn35, Lys37 and His39, with contributions from Arg12 and Lys48.

At this point we have no way of establishing experimentally how much the structure of this part of the molecule changes upon binding to the voltage-gated sodium channel. However, given that both molecules are potent cardiac stimulants, consideration of the spatial disposition of these residues in both proteins will be important in any attempt to exploit their activity in an oligopeptide or peptide mimetic.

Materials and methods

Materials

Specimens of *A. xanthogrammica* were obtained frozen from the Bodega Bay Marine Laboratories, CA. AP-B was purified from the anemone according to the method of Schweitz *et al.* [36], followed by a final purification step using reversed-phase HPLC [30].

Prior to NMR experiments, the sample was dissolved in 90% H_2O/10% ^2H_2O or ^2H_2O at a concentration of approximately 3.5 mM and pH 4.5. pH values were measured at 295 K and were uncorrected for deuterium isotope effects. ^2H_2O,

^{2}HCl and NaO^{2}H were obtained from Cambridge Isotope Laboratories (Woburn, MA).

Spectrum acquisition and analysis

All spectra were recorded on Bruker AMX-500 and AMX-600 spectrometers, with sample temperatures of 285 K, 298 K or 313 K. Experiments were recorded essentially as described in [6] with NOESY spectra [37] being acquired with mixing times of 80 ms, 160 ms, 200 ms and 250 ms in 90% H_2O/10% ^2H_2O and 80 ms and 200 ms in ^2H_2O. Slowly exchanging amide protons were identified by lyophilizing the sample from 90% H_2O/10% ^2H_2O, and then recording a series of one-dimensional and TOCSY [38] experiments immediately after dissolution in ^2H_2O at 298 K. Spectra were processed using UXNMR (Bruker) and analyzed using Felix (version 2.05, Hare Research Inc., Bothell, WA). $^3J_{HN-C\alpha H}$ coupling constants were measured from DQF-COSY spectra [39] recorded in H_2O and $^3J_{C\alpha HC\beta H}$ coupling constants from an E-COSY spectrum [40] in ^2H_2O, using the procedures described in [6].

Structural restraints

Upper-bound distance restraints were obtained from a 200 ms NOESY spectrum recorded at 298 K and processed with a 90°-shifted sine bell apodization function. The procedures used for calibration and correction of these restraints were as described in [6]. Also described therein is the procedure for defining lower-bound restraints where NOESY cross-peaks were clearly absent from the spectra; a larger number of lower-bound restraints was used for AP-B than for AP-A because they were introduced at an earlier stage of the structure calculations (when the number of upper-bound restraints was smaller). To assess the influence of these lower-bound restraints on the final structures, the simulated annealing and energy minimization steps (see below) were repeated without them. The mean pairwise rmsd for the backbone heavy atoms (N,Cα,C) of these 20 structures compared with the 20 final structures generated with lower-bound restraints included was 0.70 Å over the well-defined residues. The residues in the poorly defined loop showed greater differences, as reflected in the rmsd over all residues of 2.29 Å. The observation of a minimal effect of lower-bound restraints on well-defined regions of the structure and a greater effect on poorly defined regions is consistent with other examples [9,41].

Backbone dihedral ϕ angles were constrained as follows: −120° for ^{3}JHN-CaH>8 Hz and −60° for $^3J_{HN-C\alpha H}$<5.5 Hz. Deviations from these angles varied depending on the value of the coupling constant, the minimum deviation being 30°. Backbone dihedral restraints were not applied for $^3J_{HN-C\alpha H}$ values between 5.5 Hz and 8 Hz, except for Cys6, which had a value of 7.5 Hz. During initial structure calculations the ϕ angle for this residue converged to a positive value in a number of cases. As the intra-residue HN–CαH cross-peak for this residue was weak, and thus not consistent with a positive ϕ angle [42], the ϕ angle of Cys6 was constrained to −120±50°. $^3J_{C\alpha HC\beta H}$ coupling constants, together with $d_{\alpha\beta}(i,i)$ and $d_{N\beta}(i,i)$ NOEs from short-mixing-time NOESY spectra in ^2H_2O and H_2O, were used to determine if side chains could be placed in one of the staggered side-chain rotamer conformations (χ^1=60°, 180° and −60°) and to make stereospecific assignments [43,44]. χ^1 torsion angles were constrained to values of 60°, 180° or −60° as appropriate, with minimum deviations of 30°.

Structure calculations

Distance geometry calculations were carried out in DIANA [17] running on a ConvexC 3220 (CONVEX Computer Corp., TX). Initial structures were calculated using an incomplete data set containing only unambiguously assigned NOEs. These preliminary structures were then used to make additional NOESY cross-peak assignments based on inter-proton distances in these structures and to determine lower bound restraints [6]. Three rounds of structure calculations were carried out before the restraint list was finalized. A family of 50 structures of low energy was then generated in DIANA using three rounds of the redundant dihedral angle constraints (REDAC) strategy [45]. A further 200 structures were calculated starting from a linear template within X-PLOR [18]. The 50 lowest energy structures from DIANA and the 20 lowest energy structures originating from the linear template within X-PLOR were then refined by simulated annealing in X-PLOR, essentially as described for AP-A [6], except that additional angle-based terms were incorporated into the input files in order to set bond angles for the rings of tryptophan, tyrosine, histidine, phenylalanine and proline residues to values allowing unstrained ring closure. Finally, the structures were energy-minimized in X-PLOR with the CHARMm force-field. Energy minimization was carried out with all explicit charges neutralized (as per the templates of the GROMOS force-field [46]) and with a distance-dependent dielectric. The final set of 20 structures used for analysis were selected from the 70 CHARMm-minimized structures based on their stereochemical energies (i.e. the sum of all contributions to the calculated energy except the electrostatic term) and NOE energies. These 20 structures comprised 11 originating from DIANA and 9 from X-PLOR. Structures were analyzed using SSTRUC (D Smith, unpublished program), based on the methods of Kabsch and Sander [47]. Hydrogen bonds involving side chains were identified using the Measure HBond facility of INSIGHT (Biosym Technologies, San Diego, CA), which was also used for graphics. These 20 structures and the NMR restraints used in their determination have been deposited with the Brookhaven Protein Data Bank (accession number 1APF).

Acknowledgements: We thank Linda Legge and Rasmus Fogh for preliminary NMR analysis of AP-B, Richard Ford and Lisa Cowen for assistance with computing, David Smith for the program SSTRUC. This work was supported in part by the Australian Research Council (RSN) and an Australian Postgraduate Research (Industry) Award to SAM.

References

1. Kem, W.R. (1988). Sea anemone toxins: structure and action. In *The Biology of Nematocysts.* (Hessinger, D. & Lenhoff, H., eds), pp. 375–405, Academic Press, New York.
2. Norton, R.S. (1991). Structure and structure–function relationships of sea anemone proteins that interact with the sodium channel. *Toxicon* **29**, 1051–1084.
3. Scriabine, A., Van Arman, C.G., Morgan, G., Morris, A.A., Bennett, C.D. & Bohidar, N.R. (1979). Cardiotonic effects of anthopleurin-A, a polypeptide from a sea anemone. *J. Cardiovasc. Pharmacol.* **1**, 571–583.
4. Norton, T.R. (1981). Cardiotonic polypeptides from *Anthopleura xanthogrammica* (Brandt) and *A. elegantissima* (Brandt). *Feder. Proc.* **40**, 21–25.
5. Torda, A.E., Mabbutt, B.C, van Gunsteren, W.F. & Norton, R.S. (1988). Backbone folding of the polypeptide cardiostimulant anthopleurin-A determined by nuclear magnetic resonance, distance geometry and molecular dynamics. *FEBS Lett.* **239**, 266–270.
6. Pallaghy, P.K., Scanlon, M.J., Monks, S.A. & Norton, R.S. (1995). Three dimensional structure in solution of the polypeptide cardiac stimulant anthopleurin-A. *Biochemistry* **34**, 3782–3794.
7. Widmer, H., Billeter, M. & Wüthrich, K. (1989). The three-dimensional structure of the neurotoxin ATX Ia from *Anemonia sulcata* in aqueous solution by nuclear magnetic resonance spectroscopy. *Proteins* **6**, 357–371.

8. Fogh, R.H., Kem, W.R. & Norton, R.S. (1990). Solution structure of neurotoxin I from the sea anemone *Stichodactyla helianthus*. A nuclear magnetic resonance, distance geometry and restrained molecular dynamics study. *J. Biol. Chem.* **265**, 13016–13028.
9. Wilcox, G.R., Fogh, R.H. & Norton, R.S. (1993). Refinement of the solution structure of the sea anemone neurotoxin Sh I. *J. Biol. Chem.* **268**, 24707–24719.
10. Newcomb, R., Seriguchi, D.G., Norton, T.R. & Yasunobu, K.T. (1980). Effects of chemical modification of anthopleurin-A, a peptide heart stimulant. In *Frontiers in Protein Chemistry*. (Liu, D.T., Mamiya, G. & Yasunobu, K.T., eds), pp. 539–550, Elsevier Press, Amsterdam.
11. Gruen, L.C. & Norton, R.S. (1985). Role of aspartate residues in the cardiac stimulatory activity of anthopleurin-A. *Biochem. Int.* **11**, 69–76.
12. Gould, A.R., Mabbutt, B.C. & Norton, R.S. (1990). Structure–function relationships in the polypeptide cardiac stimulant anthopleurin-A. Effects of limited proteolysis with trypsin. *Eur. J. Biochem.* **188**, 145–153.
13. Gallagher, M.J. & Blumenthal, K.M. (1992). Cloning and expression of wild-type and mutant forms of the cardiotonic polypeptide anthopleurin B. *J. Biol. Chem.* **267**, 13958–13963.
14. Gallagher, M.J. & Blumenthal, K.M. (1994). Importance of the unique cationic residues arginine 12 and lysine 49 in the activity of the cardiotonic polypeptide anthopleurin B. *J. Biol. Chem.* **269**, 254–259.
15. Wüthrich, K. (1986). *NMR of Proteins and Nucleic Acids*. Wiley, New York.
16. Scanlon, M.J. & Norton, R.S. (1994). Multiple conformations of the polypeptide cardiostimulant anthopleurin-A. *Protein Sci.* **3**, 1121–1124.
17. Güntert, P., Braun, W. & Wüthrich, K. (1991). Efficient computation of three-dimensional protein structures in solution from NMR data using the program DIANA and the supporting programs CALIBA, HABAS and GLOMSA. *J. Mol. Biol.* **217**, 517–530.
18. Brünger, A.T. (1992). *X-PLOR Version 3.1. A System for X-ray Crystallography and NMR*. Yale University, New Haven, CT.
19. Hyberts, S.G., Goldberg, M.S., Havel, T.F. & Wagner, G. (1992). The solution structure of eglin C based on measurement of many NOEs and coupling constants and its comparison with X-ray structures. *Protein Sci.* **1**, 736–751.
20. Pallaghy, P.K., Duggan, B.M., Pennington, M.W. & Norton, R.S. (1993). Three-dimensional structure in solution of the calcium channel blocker ω-conotoxin. *J. Mol. Biol.* **234**, 405–429.
21. Chan, A.W.E., Hutchinson, E.G., Harris, D. & Thornton, J.M. (1993). Identification, classification, and analysis of beta-bulges in proteins. *Protein Sci.* **2**, 1574–1590.
22. Berndt, K.D., Güntert, P., Orbons, L.P.M. & Wüthrich, K. (1992). Determination of a high-quality nuclear magnetic resonance solution structure of the bovine pancreatic trypsin inhibitor and comparison with three crystal structures. *J. Mol. Biol.* **227**, 757–775.
23. Gooley, P.R., Blunt, J.W., Beress, L. & Norton, R.S. (1988). Effect of pH and temperature on cardioactive polypeptides from sea anemones: a ^{1}H-NMR study. *Biopolymers* **27**, 1143–1157.
24. Wishart, D.S., Sykes, B.D. & Richards, F.M. (1991). Relationship between nuclear magnetic resonance chemical shift and protein secondary structure. *J. Mol. Biol.* **222**, 311–333.
25. Wishart, D.S., Bigam, C.G., Holm, A., Hodges, R.S. & Sykes, B.D. (1995). ^{1}H, ^{13}C and ^{15}N random coil NMR chemical shifts of the common amino acids. I. Investigations of nearest-neighbor effects. *J. Biomol. NMR* **5**, 67–81.
26. Bundi, A. & Wüthrich, K. (1979). Use of amide ^{1}H-NMR titration shifts for studies of polypeptide conformation. *Biopolymers* **18**, 299–311.
27. Gould, A.R., Mabbutt, B.C., Llewellyn, L.E., Goss, N.H. & Norton, R.S. (1992). Linear and cyclic peptide analogues of the polypeptide cardiac stimulant anthopleurin-A. ^{1}H-NMR and biological activity studies. *Eur. J. Biochem.* **206**, 641–651.
28. Smith, C.K., Withka, J.M. & Regan, L. (1994). A thermodynamic scale for the β-sheet forming tendencies of the amino acids. *Biochemistry* **33**, 5510–5517.
29. Torda, A.E. & Norton, R.S. (1987). Amide proton exchange rates in cardioactive sea anemone polypeptides. *Biochem. Int.* **15**, 659–666.
30. Gould, A.R. & Norton, R.S. (1995). Chemical modification of cationic groups in the polypeptide cardiac stimulant anthopleurin-A. *Toxicon* **33**, 187–199.
31. Khera, P.K. & Blumenthal, K.M. (1994). Role of the cationic residues arginine 14 and lysine 48 in the function of the cardiotonic polypeptide anthopleurin B. *J. Biol. Chem.* **269**, 921–925.
32. Stanfield, R.L. & Wilson, I.A. (1995). Protein–peptide interactions. *Curr. Opin. Struct. Biol.* **3**, 103–113.
33. Stampe, P., Kolmakova-Partensky, L. & Miller, C. (1994). Intimations of K^+ channel structure from a complete functional map of the molecular surface of charybdotoxin. *Biochemistry* **33**, 443–450.
34. Goldstein, S.A.N., Pheasant, D.J. & Miller, D.J. (1994). The charybdotoxin receptor of a Shaker K^+ channel: peptide and channel residues mediating molecular recognition. *Neuron* **12**, 1377–1388.
35. Clackson, T. & Wells, J.A. (1995). A hot spot of binding energy in a hormone–receptor interface. *Science* **267**, 383–386.
36. Schweitz, H., *et al.*, & Lazdunski, M. (1981). Purification and pharmacological properties of eight sea anemone toxins from *Anemonia sulcata, Anthopleura xanthogrammica, Stiochactis giganticus* and *Actinodendron plumosum*. *Biochemistry* **20**, 5245–5252.
37. Anil Kumar, Ernst, R.R. & Wüthrich, K. (1980). A two-dimensional nuclear Overhauser enhancement (2D NOE) experiment for elucidation of complete proton–proton cross-relaxation networks in biological macromolecules. *Biochem. Biophys. Res. Commun.* **95**, 1–6.
38. Braunschweiler, L. & Ernst, R.R. (1983). Coherence transfer by isotropic mixing: application to proton correlation spectroscopy. *J. Magn. Reson.* **53**, 521–528.
39. Rance, M., Sørensen, O.W., Bodenhausen, G., Wagner, G., Ernst, R.R. & Wüthrich, K. (1983). Improved spectral resolution in COSY ^{1}H NMR spectra of proteins via double quantum filtering. *Biochem. Biophys. Res. Commun.* **117**, 479–485.
40. Griesinger, C., Sørensen, O.W. & Ernst, R.R. (1987). Practical aspects of the E-COSY technique. Measurement of scalar spin–spin coupling constants in peptides. *J. Magn. Reson.* **75**, 474–492.
41. Manoleras, N. & Norton, R.S. (1994). Three-dimensional structure in solution of neurotoxin III from the sea anemone *Anemonia sulcata*. *Biochemistry* **33**, 11051–11061.
42. Ludvigsen, S. & Poulsen F.M. (1992). Positive ϕ-angles in proteins by nuclear magnetic resonance spectroscopy. *J. Biomol. NMR* **2**, 227–233.
43. Wagner, G., Braun, W., Havel, T.F., Schaumann, T., Gō, N. & Wüthrich, K. (1987). Protein structures in solution by nuclear magnetic resonance and distance geometry. *J. Mol. Biol.* **196**, 611–639.
44 Hyberts, S.G., Märki, W. & Wagner, G. (1987). Stereospecific assignment of side-chain protons and characterization of torsion angles in Eglin c. *Eur. J. Biochem.* **164**, 625–635.
45. Güntert, P. & Wüthrich, K. (1991). Improved efficiency of protein structure calculations from NMR data using the program DIANA with redundant dihedral angle restraints. *J. Biomol. NMR* **1**, 447–456.
46. Van Gunsteren, W.F. & Berendsen, H.J.C. (1987). *Groningen Molecular Simulations (GROMOS)*. Biomos, Groningen, The Netherlands.
47. Kabsch, W. & Sander, C. (1983). Dictionary of protein secondary structure: pattern recognition of hydrogen-bonded and geometrical features. *Biopolymers* **22**, 2577–2637.

Received: **22 May 1995**; revisions requested: **15 Jun 1995**; revisions received: **28 Jun 1995**. Accepted: **29 Jun 1995**.